Crack Length Dependence of Mode III Delamination Using Edge Crack Torsion Test

K. J. Wong, H. A. Israr, and M. N. Tamin
Centre for Composites, Faculty of Mechanical Engineering, Universiti Teknologi Malaysia, 81310 Johor Bahru, Malaysia
Email: kjwong@mail.fkm.utm.my

***Abstract*—The objective of this study is to compare the mode III delamination behavior of edge crack torsion (ECT) specimens at different initial crack lengths, a_o. Finite element models of ECT specimens at a_o = 20 mm and 30 mm were developed based on the data from the literature. Delamination behavior was investigated using cohesive zone modeling, where cohesive elements were placed at the mid-thickness of the specimens. Results showed that the experimental and numerical force-displacement curves were comparable, with less than 10% difference in the slopes and peak loads. In addition, it was found that the cohesive zone in both models contained three elements. Furthermore, the crack front (CF) and fracture process zone (FPZ) contours revealed that the largest crack extensions were found at normalized locations of approximately 0.4 and 0.7 for a_o = 20 mm and 30 mm specimens, respectively. Finally, comparison between the fracture energy distributions and phase angle indicated that at least 30% of the crack front was mode III dominant, with phase angle of 85° and above.**

***Index Terms*—Interlaminar fracture, pure mode III, edge crack torsion, cohesive zone modeling**

I. Introduction

In the use of composite laminates in structural applications, delamination is generally recognized as one of the dominant failures. Extensive researches have been conducted to characterize mode I, mode II and mixed-mode I+II delamination behavior in laminated composites [1]-[4]. These include enhancement of the fracture toughness using Z-pins [5]-[7]. However, the studies on pure mode III delamination were comparatively much lesser. Nevertheless, the understanding of mode III delamination behavior is essential due to its contribution to edge delamination [8].

The common methods to characterize mode III delamination have been recently summarized by López-Menéndez *et al*. [9]. The available tests include split cantilever beam (SCB), simplified SCB (SSCB), modified SCB (MSCB), crack rail shear (CRS), anticlastic plate bending (ACPB), edge crack torsion (ECT), six ECT (6ECT), four point bending plate (4PBP), shear torsion bending (STB) and split-shear torsion (SST) tests. ECT test has the advantages of pure mode III delamination in the middle region of the specimen and negligible friction effects between the crack faces [10]. However, ECT test has the weaknesses of non-uniform crack propagation along the delamination front, and hence the mode III strain energy release rate is not consistent [11]. In addition, the measured fracture toughness using ECT test was found to increase with the crack length of the specimens [12], [13]. Hence, it is necessary to characterize the ECT specimens at different initial crack lengths in order to select suitable specimen's size for reliable determination of mode III fracture toughness.

The objective of this study is to analyze the crack length dependence of mode III delamination in ECT specimens. The experimental results from literature [14] were adopted. Despite finite element modeling has also been reported by the authors in [14], certain detail analyses on initial crack length dependency using cohesive zone modeling (CZM) have not been carried out. CZM is popular to simulate delamination due to its advantages of predicting both the onset and non-self-similar propagation of delamination without needing a pre-crack [15]. This study focused on the analyses with specimens at two initial crack lengths, which were a_o = 20 mm and 30 mm. Comparison were done on the cohesive zone length, damage initiation and propagation profiles, fracture energy distributions and phase angle.

II. Numerical Modeling

A. Cohesive Zone Model

In this study, cohesive element [16] was employed to simulate the delamination between the plies adjacent to the pre-crack. This type of element considers only out-of-plane stress components, and is generally known as interface element. Since the present study focused on mode III interlaminar fracture, only the formulation for delamination in tearing mode was discussed.

Consider an eight-node three-dimensional cohesive element that is subjected to loading as shown in Fig. 1. Before any delamination damage occurs, the traction separation behavior is assumed to be linear elastic. At any instant, the element is having relative displacement between the upper, $u_{III,up}$ and lower, $u_{III,low}$ nodes which is denoted as δ_{III} and is stored as the corresponding displacement at the integration point. For uncoupled shear traction, the constitutive behavior is given as:

Manuscript received January 21, 2017; revised April 24, 2017.

doi: 10.18178/ijmerr.6.3.219-225

$$t_{III} = k_{III}\delta_{III} \quad (1)$$

where t_{III} is the traction (stress) and k_{III} is the interface stiffness (stiffness per unit thickness of the cohesive element). The subscript *III* refers to the tearing mode.

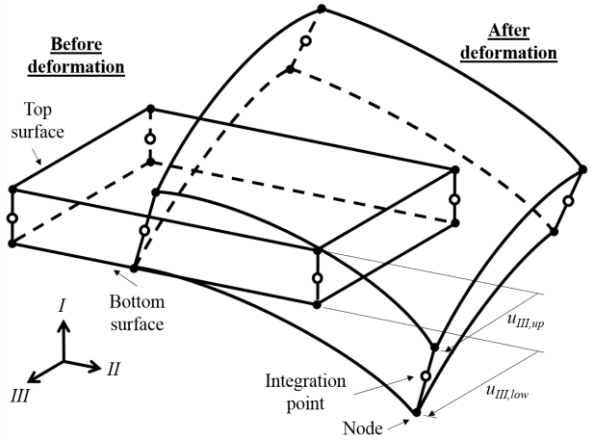

Figure 1. Schematic diagram of a three-dimensional cohesive element.

Interface damage initiation is governed by a quadratic nominal stress criterion. For pure mode III, it is written as:

$$\left\{\frac{t_{III}}{t_{u,III}}\right\}^2 = 1 \quad (2)$$

where $t_{u,III}$ is the interlaminar strength in tearing direction, which could be reduced to maximum nominal stress criterion for this particular case, where the traction ratio on the left is not squared.

Delamination starts to occur at a material point of the interface when the quotient of the nominal stress ratio reaches unity. Subsequently, damage evolution occurs. In this study, linear damage evolution law was used as described in Fig. 2.

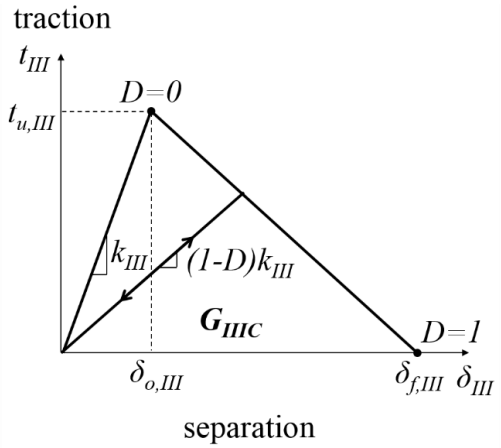

Figure 2. Schematic diagram of bilinear traction separation law.

The damage parameter, *D* for linear softening behavior is written as:

$$D = \frac{\delta_{f,III}(\delta_{III} - \delta_{o,III})}{\delta_{III}(\delta_{f,III} - \delta_{o,III})} \quad (3)$$

where $\delta_{o,III}$ and $\delta_{f,III}$ refer to the relative displacement at damage onset and total failure. Linear softening was adopted due to its simplicity and accuracy compared to other traction-separation laws such as exponential [16].

During damage evolution, the constitutive behavior of the interface is calculated based on the following equation:

$$t_{III} = (1-D)k_{III}\delta_{III} \quad (4)$$

With the computed relative displacement δ_{III} at each iteration, *D* could be calculated. The damage variable, *D* is then updated into the stiffness matrix in Equation (4) and the traction, t_{III} is updated.

Subsequently, the corresponding mode III fracture energy, G_{III} could be calculated and compared with G_{IIIC}. When the total fracture energy is equivalent to the fracture toughness (G_{III} = G_{IIIC}), *D* = 1 and the material point is completely damaged.

B. Finite Element Modeling

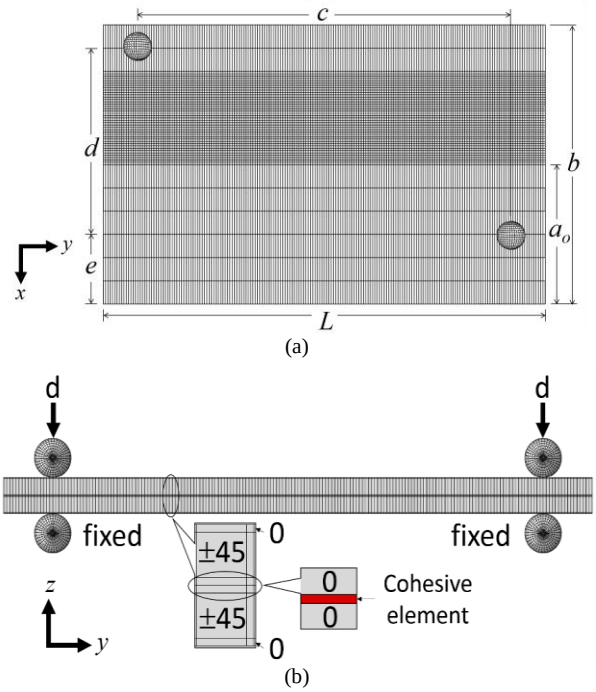

Figure 3. Finite element model of the ECT specimen: (a) top view; (b) front view.

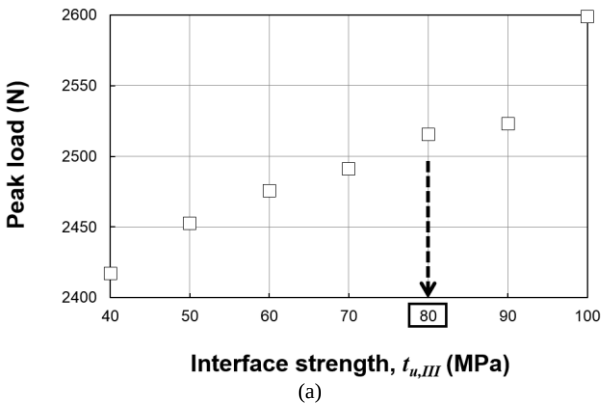

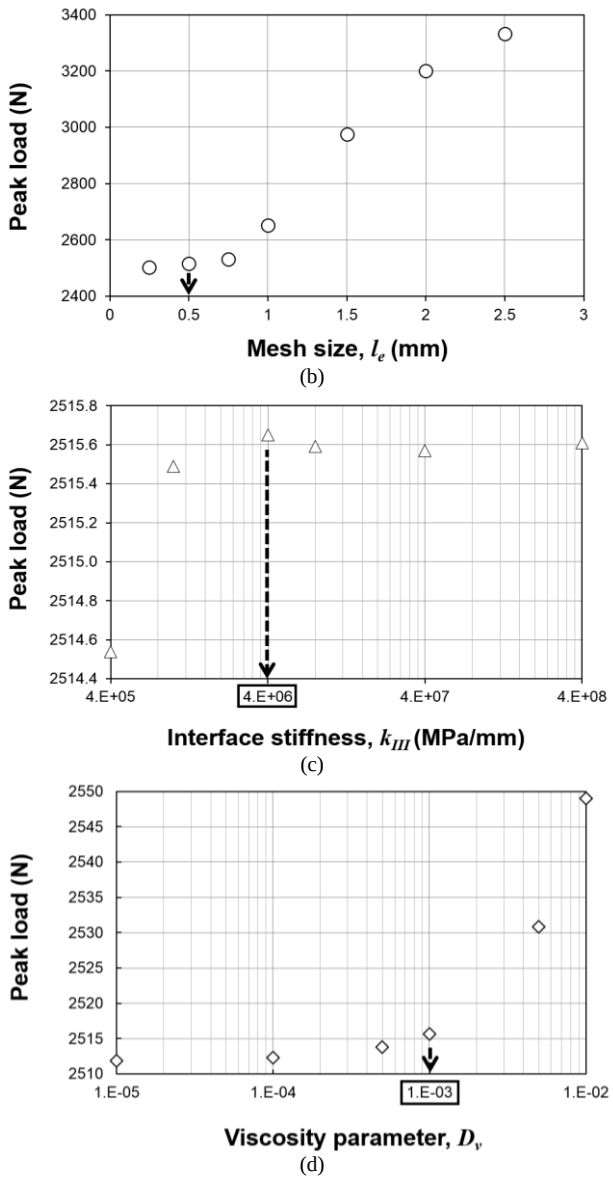

Figure 4. Comparison among (a) interface strength, (b) mesh size, (c) interface stiffness and (d) viscosity parameter and interface stiffness on the numerical peak loads [18].

TABLE I. DIMENSIONS (MM) OF THE ECT SPECIMENS USED IN THIS STUDY [14].

a_o	b	c	d	e	L
20	40	80	30	5	96
30	60	80	40	15	96

TABLE II. LAMINA PROPERTIES OF TEXIPREG T300/HS 160 REM CARBON/EPOXY COMPOSITE [14].

E_1 (GPa)	E_2 (GPa)	G_{12} (GPa)	G_{13} (GPa)	G_{23} (GPa)	v_{12}
130.0	8.2	4.1	4.1	4.1	0.27

Fig. 3 describes the finite element model of the ECT specimen. Two models were developed, with initial crack lengths of a_o = 20 mm and 30 mm. The dimensions of each model were displayed in Table I below. The composite laminate consisted of 36 layers, with the stacking sequence of $[0/(-+45)_4/(+-45)_4/0]_S$. The two bottom spheres were fixed and vertical displacement was imposed by the two upper spheres. The two mid– and outer–layers (0 plies) were modeled as individual ply, whereas all other 45 layers were modeled by one element in the thickness direction. The composite was modeled using 8-node continuum shell elements (SC8R). As for the mid-plane interface, 8-node cohesive elements (COH3D8) were prescribed to simulate the delamination behavior. Cohesive elements were modeled with 1 μm thickness to avoid interpenetration [17]. The material was Texipreg T300/HS 160 REM carbon/epoxy composite with lamina properties presented in Table II below. Table III lists the cohesive parameters used for the interface layer. The values were chosen based on parametric studies performed in the previous work [18] which were summarized in Fig. 4. From Fig. 4(a), it was found that the interface strength converged up to 80 MPa. In addition, Fig. 4(b) suggests that a mesh size of 0.5 mm and below was recommended. Furthermore, Figure 4(c) illustrates that the interface stiffness was not sensitive within the range of 4×10^5-4×10^8 MPa/mm, and hence the value of 4×10^6 MPa/mm was a reasonable choice since it was in the similar range of the values generally used by some other researchers [4], [19]-[21]. As for the viscosity parameter, Fig. 4(d) depicts that a value of 1×10^{-3} and below was a good choice for converged result. The pure-mode fracture toughness were G_{IC} = 0.25 N/mm, G_{IIC} = 0.8 N/mm and G_{IIIC} = 0.9 N/mm [13].

TABLE III. COHESIVE PARAMETERS EMPLOYED FOR THE INTERFACE LAYER [18].

Interface stiffness k_{III} (MPa/mm)	Interface strength $t_{u,III}$ (MPa)	Element size l_e (mm)	Viscosity parameter D_v
4×10^6	80	0.5	1×10^{-3}

III. RESULTS AND DISCUSSION

A. Force-Displacement Curves

Fig. 5 compares the experimental and numerical force-displacement curves of the ECT specimens. The difference in the slopes was not more than 4%, whereas less than 10% difference in the peak loads was noticed. This could serve as partial validation of the finite element models. Consequently, further analyses were carried out to investigate the delamination behavior in the ECT specimens.

B. Traction Separation Responses

Fig. 6 shows the theoretical and numerical traction separation responses of the ECT specimens at both initial crack lengths. The theoretical traction separation behavior was calculated using $k_{III} = 4\times10^6$ MPa/mm, $t_{u,III}$ = 80 MPa (Table III) and G_{IIIC} = 0.9 N/m, where the fracture toughness, G_{IIIC} is the area under the curve. Both Fig. 6(a) and Fig. 6(b) showed that the theoretical and numerical traction separation responses were identical. This has

validated the input of the cohesive zone model into the numerical analyses.

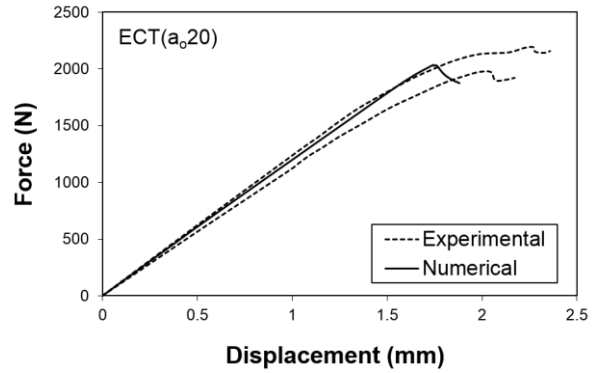

(a)

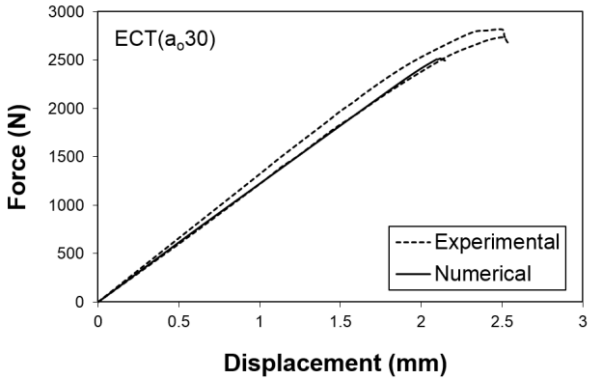

(b)

Figure 5. Experimental and numerical force-displacement curves of the ECT specimens at initial crack length of (a) 20 mm and (b) 30 mm.

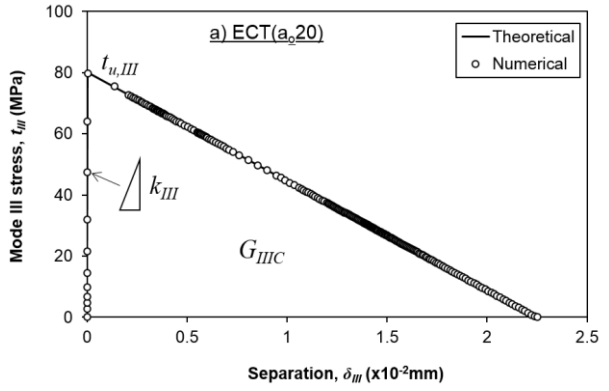

(a)

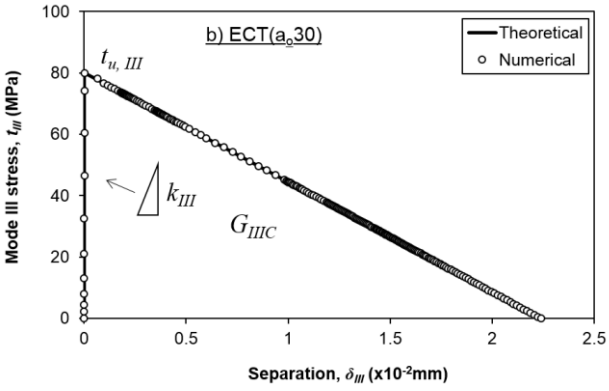

(b)

Figure 6. Theoretical and numerical traction separation responses of the ECT specimens with (a) a_o = 20 mm and (b) a_o = 30 mm.

C. Cohesive Zone Length

Cohesive zone length, $L_{cz,f}$ is the distance between the first element that has attained total damage (D = 1) and the crack tip element which damage is just initiated (D = 0). Within the cohesive zone, it is essential to have sufficient number of cohesive elements to ensure satisfactory simulation results. The minimum number of cohesive elements, N_e, is related to $L_{cz,f}$ and l_e by the following equation:

$$N_e = \frac{L_{cz,f}}{l_e} \tag{5}$$

Fig. 7 shows the stress distribution of the first fully developed cohesive zone of the ECT specimens. It is noticed that $L_{cz,f}$ was 1.5 mm in both cases. In other words, there were 3 cohesive elements within the cohesive zone. This is similar to the finding by other researchers, where at least 2 – 3 cohesive elements are necessary for reliable simulations [21], [22].

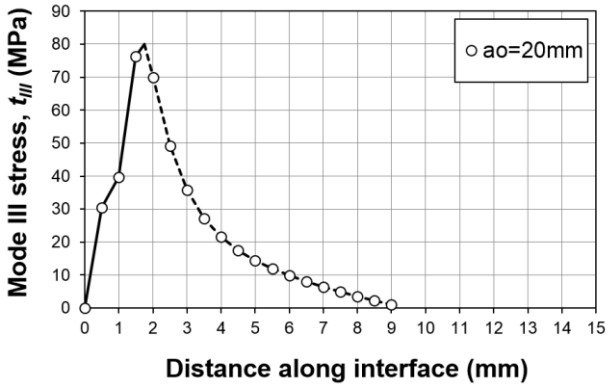

(a)

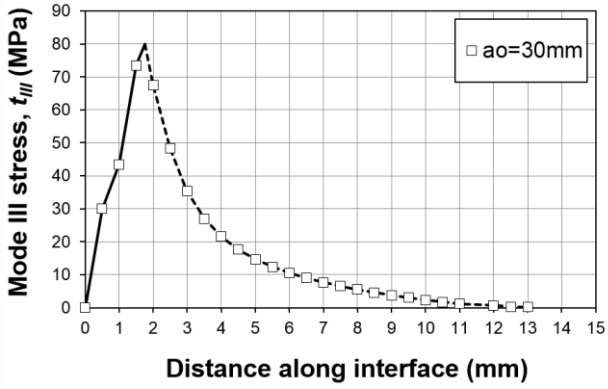

(b)

Figure 7. Stress distribution of the first fully developed cohesive zone of ECT specimens at initial crack length of (a) 20 mm and (b) 30 mm.

D. Crack Front and Fracture Process Zone Profiles

The Crack Front (CF) indicates the region where the cohesive elements have experienced total failure (D = 1). The Fracture Process Zone (FPZ) refers to the region where the damage has initiated in the cohesive elements ($0 < D < 1$). The CF and FPZ contours of the ECT specimens were displayed in Fig. 8. Both figures showed that the crack propagation was not uniform. This is consistent with what was reported in the literature [6], [7]. Nevertheless, the CF of the a_o = 20 mm specimen was

found to be more uniform compared to the a_o = 30 mm specimen. This suggested that a_o = 20 mm could be a better choice for ECT test. In addition, in the a_o = 20 mm specimen, damage was firstly initiated and propagated at $y/L \approx 0.4$. On the other hand, it was approximately 0.7 in the a_o = 30 mm specimen. At the peak load, the crack has propagated (D = 1) for approximately 1.9 mm and 2.8 mm in a_o = 20 mm and a_o = 30 mm ECT specimens, respectively. In addition, damage has initiated ($0 < D < 1$) for 2.5 mm and 3.2 mm in both specimens.

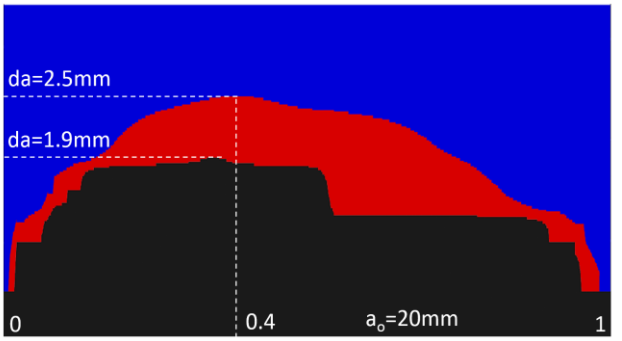

(a)

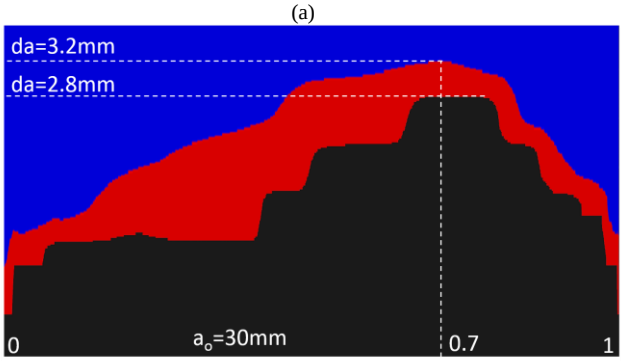

(b)

Figure 8. Crack front and fracture process zone along the crack front of ECT specimens at initial crack length of (a) 20 mm and (b) 30 mm.

E. Fracture Energy Distributions

The fracture energy distributions, G_C along the crack front at the peak load were presented in Fig. 9. In order to investigate the mode III component in the delamination, the phase angle, $\theta = \tan^{-1}(\delta_{III}/\delta_{II})$ was also plotted, where δ_{II} and δ_{III} were the mode II and mode III separations, respectively. Theoretically, pure mode III was only attained when $\delta_{II} = 0$ ($\theta = 90^o$). However, it could be noticed that this was not achieved in both specimens. Nevertheless, mode III was still observed to be dominant along a comparatively large region. Within the constant fracture energy region (G_C = 0.9 N/mm), mode III was dominated ($\theta \geq 85^o$) within the normalized distance of 0.33 – 0.65 and 0.27 – 0.65 for a_o = 20 mm and a_o = 30 mm specimens, respectively. This implied that at least 30% of the crack front was mode III dominant. In a_o = 20 mm and a_o = 30 mm specimens, the largest phase angle was attained at the normalized distance of 0.65 and 0.35, respectively. It is worth to note that the normalized distance of 0.65 is also equivalent to 0.35 from the right. These observations highlighted that it is reasonable to regard ECT test as a pure mode III fracture toughness test. Nevertheless, the non–uniform crack propagation and the initial crack length dependence of ECT specimens need to be taken into consideration when conducting ECT tests.

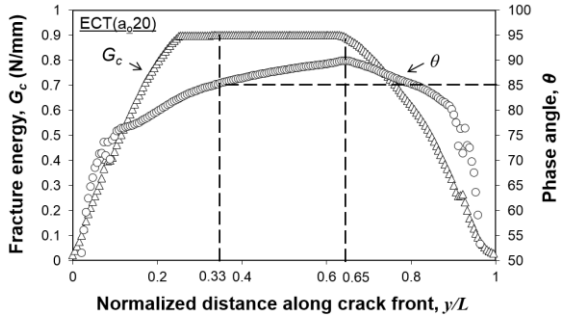

(a)

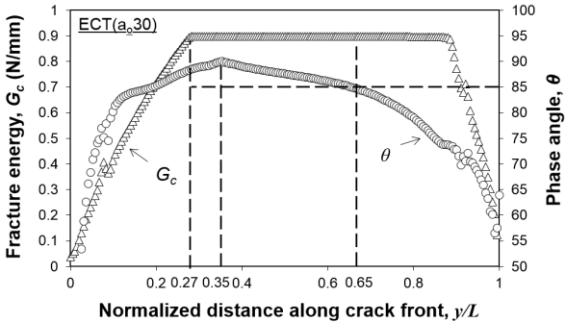

(b)

Figure 9. Fracture energy and strain distributions along the crack front of ECT specimens at initial crack length of (a) 20 mm and (b) 30 mm.

IV. Concluding Remarks and Future Recommendations

In this study, the mode III delamination behavior of ECT specimens at initial crack lengths of a_o = 20 mm and 30 mm were simulated using cohesive elements. Good comparison was found between the experimental and numerical force-displacement curves, with less than 10% difference in the slopes and peak loads. In addition, at both initial crack lengths, there were three elements in the cohesive zone. Furthermore, the crack front (CF) and fracture process zone (FPZ) contours indicated that the largest crack initiation and propagation were observed at normalized locations, $y/L \approx 0.4$ and 0.7 for a_o = 20 mm and 30 mm specimens, respectively. Finally, the fracture energy distributions and phase angle plots revealed that mode III dominant region (phase angle $\geq 85^o$) was at least 30% of the distance along the crack front.

The numerical analyses from this study provided the information of crack initiation and propagation in ECT specimens, which are not easily measured experimentally. This enabled proper selection of the specimens' size prior to experimental testing.

This work could be extended to the experimental studies of the mode III delamination using ECT test with different composite laminates. Based on the numerical simulation results obtained from this study, it is suggested that the ECT specimens are to be tested at a_o = 20 mm. Subsequently, numerical simulations could be carried out again using the suggested cohesive parameters.

Not only that, further works could also be considered on the mixed-mode delamination that involves mode III components. Typically, six point bending plate (6PBP) and eight point bending plate (8PBP) tests for mixed-mode II+III and mixed-mode I+III which were developed based on ECT.

ACKNOWLEDGEMENTS

This work is supported by Ministry of Higher Education Malaysia and Universiti Teknologi Malaysia through Fundamental Research Grant Scheme (FRGS) No. 4F591.

REFERENCES

[1] Y. Zhao, W. Liu, L. K. Seah, and G. B. Chai, "Delamination growth behavior of a woven E-glass/bismaleimide composite in seawater environment," *Composites Part B: Engineering*, vol. 106, pp. 332-343, 2016.
[2] L. R. LeBlanc and G. LaPlante, "Experimental investigation and finite element modeling of mixed-mode delamination in a moisture-exposed carbon/epoxy composite," *Composites Part A: Applied Science and Manufacturing*, vol. 81, pp. 202-213, 2016.
[3] Y. Liu, C. Zhang, and Y. Xiang, "A critical plane-based fracture criterion for mixed-mode delamination in composite materials," *Composites Part B: Engineering*, vol. 82, pp. 212-220, 2015.
[4] L. Zhao, Y. Gong, J. Zhang, Y. Chen, and B. Fei, "Simulation of delamination growth in multidirectional laminates under mode I and mixed mode I/II loadings using cohesive elements," *Composite Structures*, vol. 116, pp. 509-522, 2014.
[5] F. Pegorin, K. Pingkarawat, S. Daynes, and A. P. Mouritz. "Influence of Z-pin length on the delamination fracture toughness and fatigue resistance of pinned composites," *Composites Part B: Engineering*, vol. 78, pp. 298-307, 2015.
[6] F. Pegorin, K. Pingkarawat, and A. P. Mouritz. "Comparative study of the mode I and mode II delamination fatigue properties of Z-pinned aircraft composites," *Materials & Design*, vol. 65, pp. 139-146, 2015.
[7] H. S. Huang and A. M. Waas, "Quasi-static mode II fracture tests and simulations of Z-pinned woven composites," *Engineering Fracture Mechanics*, vol. 126, pp. 155-165, 2014.
[8] S. S. Wang, "Fracture Mechanics for delamination problems in composite materials," *Journal of Composite Materials*, vol. 17, no. 3, pp. 210-223, 1983.
[9] A. López-Menéndez, J. Viña, A. Argüelles, S. Rubiera, and V. Mollón, "A new method for testing composite materials under mode III fracture," *Journal of Composite Materials*, vol. 50, no. 28, pp. 3973-3980, 2016.
[10] D. Zhao and Y. Wang, "Mode III fracture behavior of laminated composite with edge crack in torsion," *Theoretical and Applied Fracture Mechanics*, vol. 29, no. 2, pp. 109-123, 1998.
[11] G. Browning, L. A. Carlsson, and J. G. Ratcliffe, "Redesign of the ECT test for mode III delamination testing. Part I: Finite element analysis," *Journal of Composite Materials*, vol. 44, no. 15, 2010.
[12] F. A. Mehrabadi and M. Khoshravan, "Mode III interlaminar fracture and damage characterization in woven fabric-reinforced glass/epoxy composite laminates," *Journal of Composite Materials*, vol. 47, no. 13, pp. 1583-1592, 2012.
[13] F. A. Mehrabadi, "Analysis of pure mode III and mixed mode (III+II) interlaminar crack growth in polymeric woven fabrics," *Materials & Design*, vol. 44, pp. 429-437, 2013.
[14] A. B. de Morais, A. B. Pereira, M. F. S. F. de Moura, and A. G. Magalhães, "Mode III interlaminar fracture of carbon/epoxy laminates using the edge crack torsion (ECT) test," *Composites Science and Technology*, vol. 69, no. 5, pp. 670-676, 2009.
[15] D. Xie and A. M. Waas, "Discrete cohesive zone model for mixed-mode fracture using finite element analysis," *Engineering Fracture Mechanics*, vol. 73, no. 13, pp. 1783-1796, 2006.
[16] P. P. Camanho, C. G. Davila, and M. F. S. F. de Moura, "Numerical simulation of mixed-mode progressive delamination in composite materials," *Journal of Composite Materials*, vol. 37, no. 16, pp. 1415-1438, 2003.
[17] B. F. Sørensen, S. Goutianos, and T. K. Jacobsen, "Strength scaling of adhesive joints in polymer–matrix composites," *International Journal of Solids and Structures*, vol. 46, no. 3–4, pp. 741-761, 2009.
[18] K. J. Wong, H. A. Israr, and M. N. Tamin, "Cohesive zone modeling of mode III delamination using edge crack torsion test," presented at the Symposium on Damage Mechanisms in Materials and Structures, Bangi, Malaysia, August 9, 2016.
[19] L. Zhao, Y. Gong, T. Qin, S. Mehmood, and J. Zhang, "Failure prediction of out-of-plane woven composite joints using cohesive element," *Composite Structures*, vol. 106, pp. 407-416, 2013.
[20] V. Mollón, J. Bonhomme, A. M. Elmarakbi, A. Argüelles, and J. Viña, "Finite element modelling of mode I delamination specimens by means of implicit and explicit solvers," *Polymer Testing*, vol. 31, no. 3, pp. 404-410, 2012.
[21] P. W. Harper, L. Sun, and S. R. Hallett, "A study on the influence of cohesive zone interface element strength parameters on mixed mode behaviour," *Composites Part A: Applied Science and Manufacturing*, vol. 43, no. 4, pp. 722-734, 2012.
[22] A. Turon, C. G. Dávila, P. P. Camanho, and J. Costa, "An engineering solution for mesh size effects in the simulation of delamination using cohesive zone models," *Engineering Fracture Mechanics*, vol. 74, no. 10, pp. 1665-1682, 2007.

King J. Wong graduated with a Ph.D. in Mechanics from Université de Bourgogne, Burgundy, France in 2013. His doctoral thesis was on Moisture Absorption Characteristics and Effects on Mechanical Behaviour of Carbon/Epoxy Composite: Application to Bonded Patch Repairs of Composite Structures.

He is currently a senior lecturer in the Faculty of Mechanical Engineering, Universiti Teknologi Malaysia (UTM). He is a member of the research team at the Computational Solid Mechanics Laboratory (CSMLab), UTM and also an associate member of the Centre for Composites (CfC), UTM. His has published several ISI listed journals such as Thickness-dependent Non-Fickian Moisture Absorption in Epoxy Molding Compounds, Impact Resistance of Short Bamboo Fibre Reinforced Polyester Concretes and Fracture Characterisation of Short Bamboo Fibre Reinforced Polyester Composites. His research interests include durability of engineering materials, adhesive joints, delamination of composite laminates and computational solid mechanics.

Dr. Wong is a registered member of Board of Engineers Malaysia (BEM).

Haris A. Israr was born on 5th October 1983 in Kedah, Malaysia. He received a B.Eng (Mechanical-Aeronautics) degree from Universiti Teknologi Malaysia (UTM) in 2007 and a MSc. degree in Aerospace Mechanics and Avionics from Université de Toulouse (ISAE), France in 2010. Then, he completed a Ph.D. study in Mechanical Engineering and Mechanics of Materials at the same institution (ISAE, France). His doctoral dissertation was on Crashworthiness Behavior of CFRP Composite Laminates.

He is currently a senior lecturer in the Faculty of Mechanical Engineering, UTM. He is also an associate member of Center for Composite (CFC), UTM and Computational Solid Mechanics Laboratory (CSMLab), UTM. His research interests are mostly related to composite structure i.e. impact damage, crashworthiness and ageing behavior, investigated both experimentally and numerically. He has authored several international journals, conference proceedings and book chapter related to damage mechanisms of composite structure as well as the development of finite element modelling. His current research program includes projects on Energy Dissipation Behavior of Eco-Composite which is funded by the Ministry of Education, Malaysia.

Dr. Israr is a graduate member of Board of Engineer (BEM), Malaysia and Institution of Engineer (IEM), Malaysia and recently has been appointed as one of the editors for Journal of Transport System Engineering (JTSE) under UTM Press Publisher.

Mohd N. Tamin graduated with a Ph.D. in Mechanical Engineering and Applied Mechanics from University of Rhode Island, Kingston, RI, USA in 1997. His doctoral dissertation was on Fatigue Damage Mechanisms in SiC/Ti Metal Matrix Composites.

He is currently a professor in the Faculty of Mechanical Engineering, Universiti Teknologi Malaysia (UTM). His research team at the Computational Solid Mechanics Laboratory (CSMLab), UTM, is actively working on the development of constitutive and damage-based models for ductile and fibrous composite laminates. He has written a research book on Solder Joint Reliability Assessment: Finite Element Simulation Methodology (Switzerland: Springer, 2014). His current research program includes projects on Fractal Fracture Mechanics Applications for Fatigue Crack Propagation, Fatigue Damage Assessment of CFRP Composite Laminates, and Fatigue of Steel Wire Ropes. These projects are funded by the Ministry of Education, Malaysia, The Aerospace Malaysia Innovation Center (AMIC), Malaysia, and Kiswire (Korea) R&D Center, respectively.

Prof. Tamin is a registered Chartered Engineer (CEng) and member of IMarEST and IEEE (CPMT Chapter).